

# 1 **Formation of Alfvénic resonance layers in magnetic reconnection**

2 L. J. Li, L. P. Tian, and Z. W. Ma\*

3 *Institute for Fusion Theory and Simulation, Zhejiang University, Hangzhou 310027,*  
4 *China*

5  
6 **Abstract:** In the framework of two-dimensional incompressible MHD, we investigate  
7 the formation of Alfvénic resonance layers with different super-Alfvénic shear flows.  
8 It is found that Alfvénic resonance layers are formed in the inflow region. The  
9 Alfvénic layers are located where the flow velocity equals to the local Alfvén speed  
10 and slowly drift away from the current sheet region as magnetic island develops. The  
11 presence of Alfvénic resonance layers can sufficiently suppress the magnetic  
12 reconnection. The suppressing effect depends largely on the intensity of the current  
13 density in Alfvénic resonance layers and the distance between two layers. As the  
14 velocity of the shear flow increases or the thickness of the shear flow reduces, the pair  
15 of Alfvénic layers tend to approach each other. The peak reconnection rate depends  
16 nonmonotonically on both the thickness  $a_v$  and the velocity  $v_0$  of the shear flow.  
17 The maximum of the peak reconnection rate occurs at  $v_0 = 1.2$  for the fixed  
18 thickness  $a_v = 0.8$  and  $a_v = 1.3$  for the fixed velocity  $v_0 = 1.6$ . There are thresholds  
19 for both the thickness and the velocity of the shear flow. Above the velocity threshold  
20  $v_0 \sim 1.5$  or below the thickness threshold  $a_v \sim 0.85$ , the peak reconnection rate is  
21 less than that of the case without an initially imposed shear flow and two magnetic  
22 islands are usually generated due to formation of Alfvénic resonance layers near the  
23 central current sheet.

24  
25 **Keywords:** Magnetic reconnection, shear flows, Alfvénic resonances, incompressible  
26 MHD

27  
28 \*) Corresponding author: zwma@zju.edu.cn

29

## 30 **1. Introduction**

31 Magnetic reconnection is an important process in space and laboratory plasmas,  
32 which provides a key mechanism for the energy conversion from the solar wind to the  
33 magnetosphere [Dungey, 1961]. It's widely regarded as magnetic reconnection can  
34 explain many observed phenomena in space, such as solar flare [Giovanelli, 1946]  
35 and magnetospheric substorm [Angelopoulos *et al.*, 2008].

36 Strong shear flow and magnetic shear generally coexist in the space environment,  
37 e.g., in the solar atmosphere and at the dayside magnetopause. The Kelvin-Helmholtz  
38 (KH) instability can be stimulated in the presence of a shear flow; the resistive tearing  
39 instability or magnetic reconnection occurs when the magnetic field is reversed with a  
40 small spatial scale. The shear flow in a magnetized plasma could have a significant  
41 impact on magnetic reconnection. Many researchers have investigated the effects of  
42 the shear flow on the resistive tearing mode [Ofman *et al.*, 1991,1993; Chen and  
43 Morrison, 1990a, b; Li and Ma, 2010, Zhang *et al.*, 2011, Wu and Ma, 2014] and the  
44 Kelvin-Helmholtz instability [Miura, 1982; Chen *et al.*, 1997; Shen and liu, 1999].

45 Super-Alfvénic shear flow may lead to the development of the KH instability, the  
46 growth rate could highly be enhanced [La Belle-Hamer *et al.*,1988]. Liu and Hu [1988]  
47 developed a new reconnection model so called a vortex-induced reconnection. If there  
48 is a strong velocity shear in the current sheet, the excited KH instability could produce  
49 large scale flow vortices. Consequently, the magnetic reconnection takes place due to  
50 the magnetic field line twist associated with flow vortices. The KH instability, in  
51 general, leads to a wavy current sheet and an "S" shape of magnetic islands. A fast  
52 shock can be formed due to the interaction between the strong shear flow and the  
53 magnetic island [Shen *et al.*, 2000]. Knoll *et al.* [2002] found that the peak  
54 reconnection rate with a super-Alfvénic shear flow is not a function of the resistivity  
55 instead of a function of the initial shear flow. For a particular resistivity, the peak  
56 reconnection rate increases with increase of the super-Alfvénic shear flow. But,  
57 Alfvénic resonances can occur in the place where the flow velocity matches the local  
58 Alfvénic speed [Hurricane *et al.*, 1995; Wang *et al.*, 1998]. The generation of Alfvénic  
59 layers could strongly suppress the development of magnetic reconnection.

60 However, in the previous studies about the role of super-Alfvénic shear flows on  
61 magnetic reconnection the ratio  $R = a_B/a_V$  is assumed to be one, where  $a_B$  and  $a_V$   
62 are the thickness of the current sheet and the shear flow, respectively. Wang et al.  
63 [1998] analytically and numerically investigated the Alfvénic resonance effects on  
64 magnetic reconnection with the plasma rotation boundary. Alfvénic resonance layer  
65 formation with super-Alfvénic shear flows are also investigated based on the  
66 compressible MHD simulation model, but it is not systematically analyzed [Li and Ma,  
67 2012]. In the present paper, we will systematically investigate different super-Alfvénic  
68 shear velocities and shear thicknesses. It's found that Alfvénic resonance layers  
69 formed in the inflow region can largely affect dynamic processes of magnetic  
70 reconnection. The paper is organized as follows: In section 2, we present the  
71 equations and numerical model. Section 3 shows the results of the simulation. The  
72 summary and discussion are given in section 4.

73

## 74 2. Equations and Numerical Model

75 The incompressible 2-dimensional MHD model is employed to investigate the  
76 instability with different super-Alfvénic shear flows. In our simulations, the Cartesian  
77 coordinate system is used, in which all quantities remain invariant in the  $z$  direction,  
78 that is  $\partial/\partial z = 0$ . The reduced MHD equations are as follows:

$$79 \quad \frac{\partial \psi}{\partial t} = -\mathbf{v} \cdot \nabla \psi + \frac{1}{S} \nabla^2 (\psi - \psi_0) \quad (1)$$

$$80 \quad \frac{\partial \omega}{\partial t} = -\mathbf{v} \cdot \nabla \omega + \mathbf{B} \cdot \nabla J_z + \frac{1}{S_v} \nabla^2 (\omega - \omega_0) \quad (2)$$

$$81 \quad \omega = \nabla^2 \phi \quad (3)$$

$$82 \quad J_z = \nabla^2 \psi \quad (4)$$

83 where  $\mathbf{v} = \hat{z} \times \nabla \phi$ ,  $\mathbf{B} = \hat{z} \times \nabla \psi$  with the assumptions  $B_z = 0$  and  $v_z = 0$ .  $\omega$ ,  $J_z$   
84 are the flow vorticity and the current in the  $z$  direction, respectively.  $S = \tau_R/\tau_A$  is  
85 the Lundquist number and  $S_v = \tau_v/\tau_A$  is the Reynolds number, where  $\tau_A = a/v_A$  is

86 the Alfvénic time,  $v_A = B_0 / (4\pi\rho)^{1/2}$  is the Alfvénic velocity,  $\tau_R = 4\pi a^2 / \eta c^2$  is the  
87 resistive diffusion time,  $\tau_\nu = \rho a^2 / \nu$  is the viscous diffusion time,  $a$  is the  
88 normalization unit of the length,  $c$  is the speed of light in the free space,  $\eta$  is the  
89 resistivity and  $\nu$  is the viscosity. All variables have been normalized as follows:  
90  $\mathbf{x}/a \rightarrow \mathbf{x}$ ,  $\mathbf{B}/B_0 \rightarrow \mathbf{B}$ ,  $t/\tau_A \rightarrow t$ ,  $\mathbf{v}/v_A \rightarrow \mathbf{v}$ ,  $\psi/aB_0 \rightarrow \psi$ ,  $\phi/av_A \rightarrow \phi$ . In the  
91 incompressible plasma system, the density  $\rho$  is assumed to be uniform and always  
92 set to be 1. It should be emphasized that  $S$  and  $S_\nu$  are constant.

93 Equations above are solved with fourth-order Runge-Kutta method in time and  
94 second-order finite difference method in space. The system size is  $L_x = [-2, 2]$  and  
95  $L_y = [-4, 4]$  with  $502 \times 1001$  uniform grid points in the  $x$  and  $y$  direction.  
96 Periodic boundary conditions are imposed at  $x = \pm L_x$ , while free boundary conditions  
97 are applied on  $y = \pm L_y$ . The initial magnetic field and plasma flow profiles are  
98 chosen to be the following forms:

$$99 \quad \mathbf{B}(y) = B_0 \tanh(y/a_B) \hat{x} \quad (5)$$

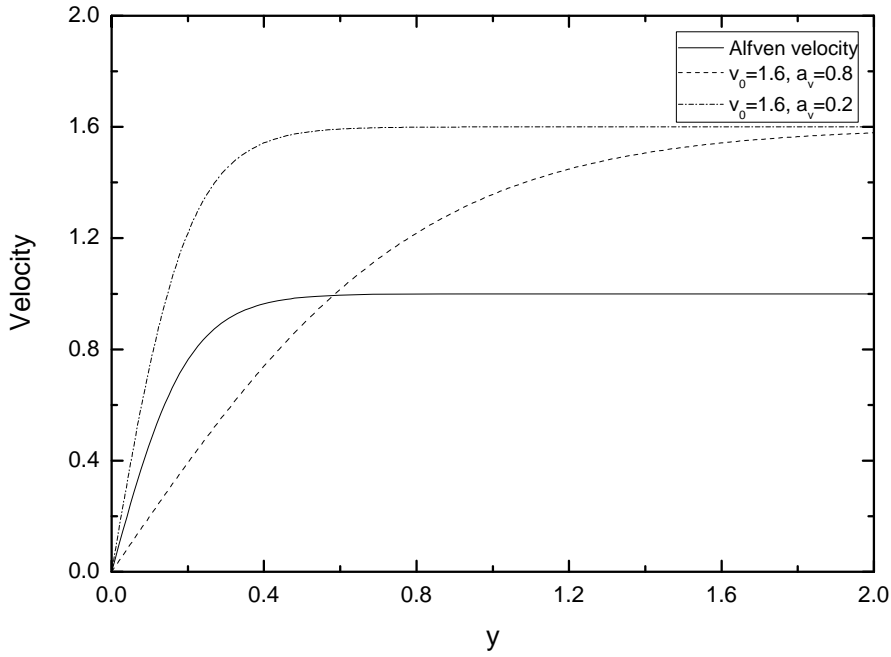
$$100 \quad \mathbf{v}(y) = -v_0 \tanh(y/a_\nu) \hat{x} \quad (6)$$

101 where  $a_\nu$  and  $a_B$  are the half thickness of the current sheet and the shear flow,  $B_0$   
102 and  $v_0$  are the asymptotic values of the magnetic field and the shear flow velocity,  
103 respectively. We set  $S = 1000$ ,  $S_\nu = 10000$ ,  $a_B = 0.2$ , and  $B_0 = 1.0$  to be fixed  
104 throughout this paper whereas  $a_\nu$  and  $v_0$  are varied with  $a_\nu \geq 0.6$  and  $v_0 \geq 1$ .

105 In our simulation, the magnetic reconnection rate  $E_r$  can be diagnosed by using  
106 the following method:

$$107 \quad E_r = \eta [J(px) - J(po)] \quad (7)$$

108 Where  $px$  and  $po$  are the location of X and O points, respectively.



110

111 Figure 1. The profiles of the Alfvénic velocity (solid line) calculated from the local magnetic  
 112 field and the shear flows for  $a_v = a_B = 0.2$  (dash-dotted line) and  $a_v = 4a_B = 0.8$  (dashed  
 113 line).

114

### 115 3. Simulation results

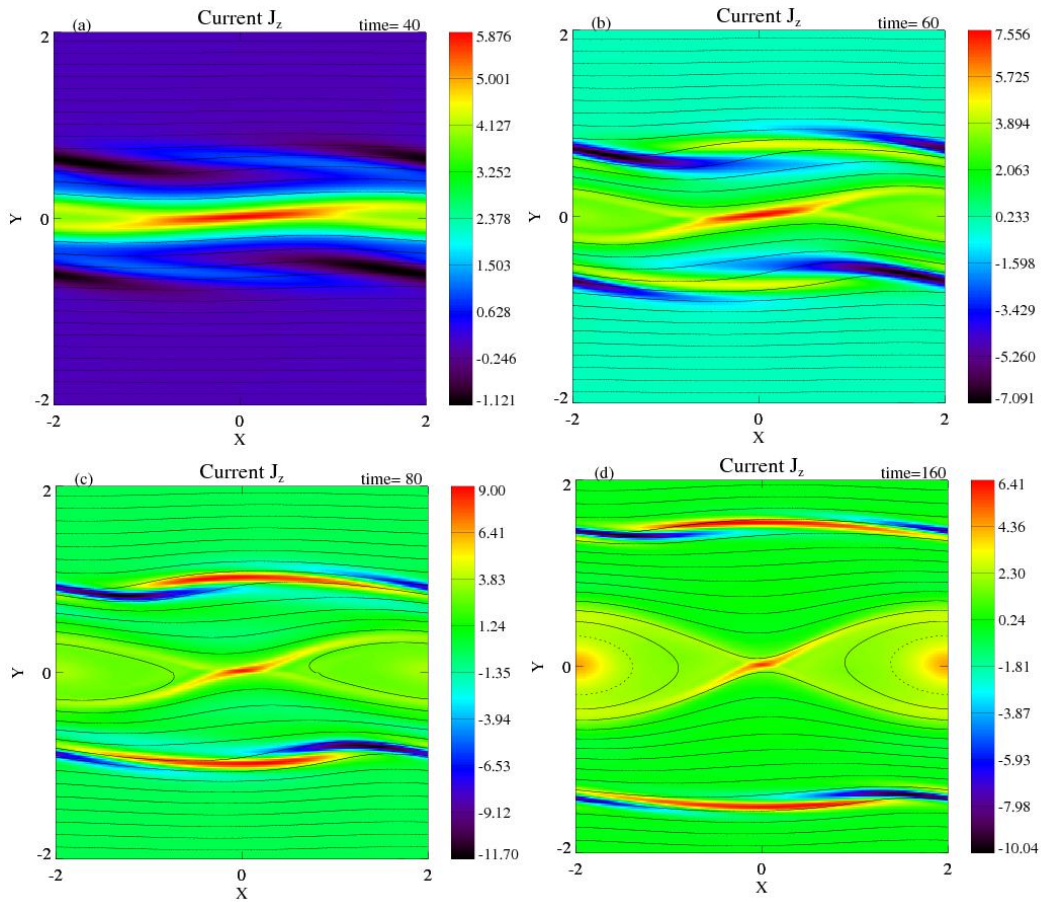
116 The formation of Alfvénic resonances can occur in such configuration where the  
 117 flow velocity matches the local Alfvénic speed, which can indicate from the follow  
 118 equation:

$$119 \quad \frac{d}{dy} \left[ \mu_0 \rho (\omega^2 - k_x^2 v_A^2) \frac{d\tilde{\xi}_y}{dy} \right] - k_x^2 \mu_0 \rho (\omega^2 - k_x^2 v_A^2) \tilde{\xi}_y = 0 \quad (8)$$

120 The equation (8) is derived in the incompressible MHD model [Bellan, 1994].

121 The condition of Alfvénic resonances is satisfied when the thickness of  
 122 super-Alfvénic shear flow is wider than that of the current sheet (the dashed line as  
 123 shown in Figure 1). Most of previous works assume that  $a_v$  is equal to  $a_B$ , the  
 124 condition can't be met (the dash-dotted line in Figure 1). Thus, the Alfvénic resonance

125 layers in the presence of super-Alfvénic shear flow are seldom reported during  
 126 magnetic reconnection. Also, we can easily find that the resonance condition, where  
 127 the velocity initially imposed shear flow matches the local Alfvénic speed, can be well  
 128 satisfied for the  $v_0 > 1.0$  and  $a_v > a_B = 0.2$  cases. The resonance position moves  
 129 away from the current sheet as the initial shear flow thickness  $a_v$  increases for a  
 130 given velocity  $v_0$ .



131  
 132 Figure 2. Contour plots of the current density distributions with magnetic field lines for  
 133  $a_v = 4a_B = 0.8$  and  $v_0 = 1.6$  at four different developed stages of magnetic reconnection.

134

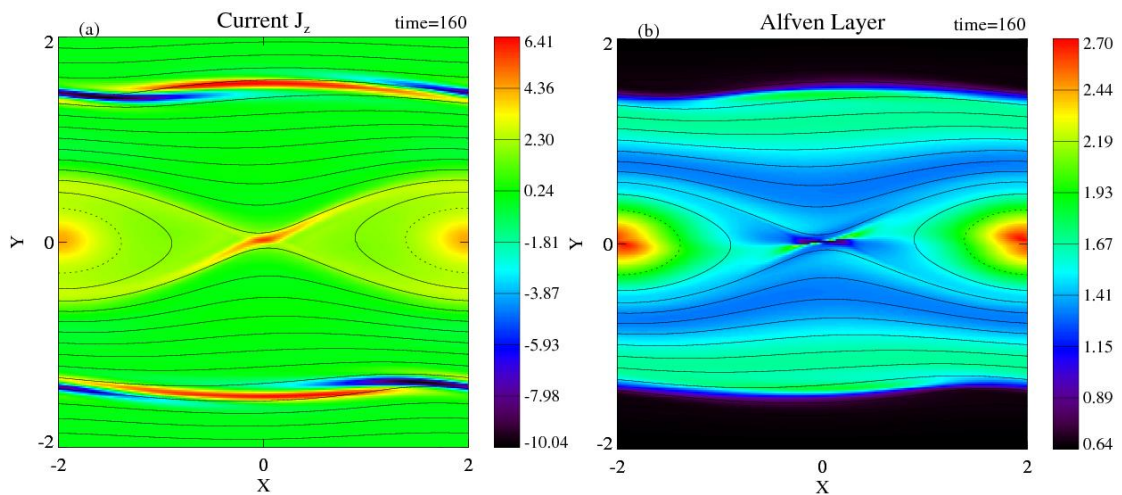
135 **A. Effects of asymptotic flow velocities for  $a_v = 4a_B = 0.8$**

136 In this section, we consider the cases with fixing the thickness of the shear flow  
 137  $a_v = 4a_B = 0.8$  and varying its initial asymptotic flow velocity in the range  $[1.0, 2.0]$ .

138 We mainly focus on the influence of initial asymptotic flow velocity on the magnetic

139 reconnection evolution and the formation of resonance layers.

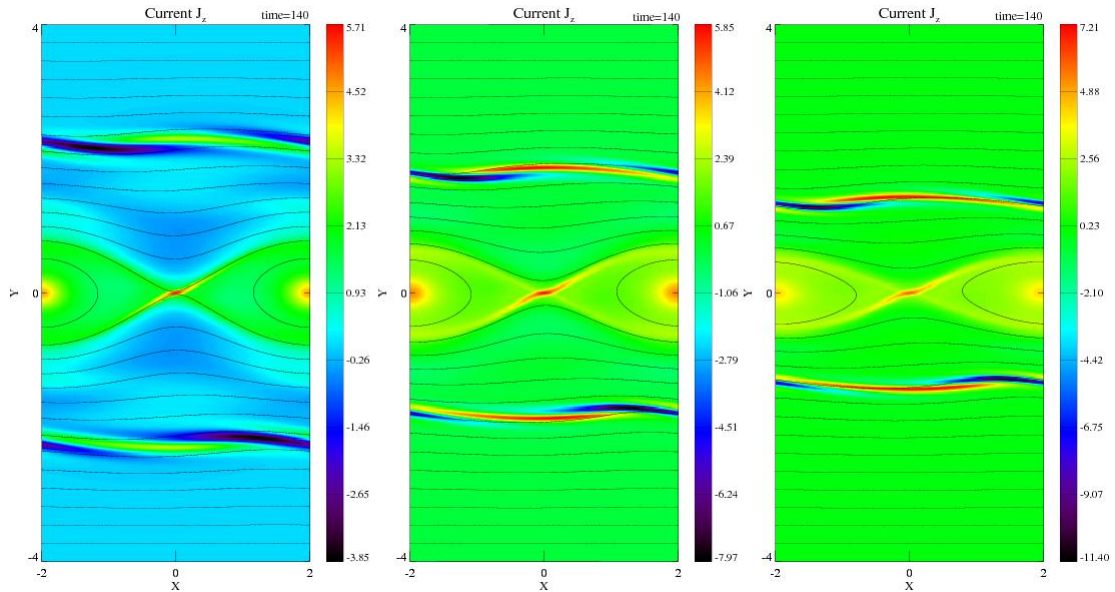
140 Figure 2 shows the distributions of the current density at different stage for  
141  $a_v = 4a_B$  and  $v_0 = 1.6$ . It's worth noting that only the half simulation domain of Y  
142 direction is plotted in Figure 2a-d. The four distinct phases are the “early rapidly  
143 changing phase”, the “most rapidly changing phase”, the “phase with maximum  
144 reconnection rate”, and the “nearly saturated phase”, respectively. In Figure 2a-b, we  
145 observe that the current sheet become wavy due to the KH disturbance, which is  
146 similar to those of the incompressible and compressible cases [Liu and Hu, 1988; Pu  
147 *et al*, 1990]. It's interesting to note that a pair of layers appears in Figure 2b and  
148 gradually becomes obvious, the initial locations of the Alfvénic resonance layers are  
149 about  $y = \pm 0.6$  where the initial shear velocity equals to Alfvénic speed which can  
150 obviously get from Figure 1. Meanwhile, the magnetic islands have the shape of “S”.  
151 As the island develops, the two resonance layers move away from each other slowly  
152 and finally become nearly stationary when the reconnection enters the saturated phase,  
153 as shown in figure 2c and figure 2d, then it exhibits a conventional reconnection  
154 configuration. The current density in the Alfvénic resonance layers increases quickly  
155 when the magnetic reconnection enters the “most rapidly changing phase”, then  
156 slowly decreases, and finally tends to a steady state in the “nearly saturated phase”.



157  
158 Figure 3. Contour plots of (a) the current density distribution (b) the ratio of the local Alfvénic  
159 speed and the flow velocity for  $v_0 = 1.6$ ,  $a_v = 4a_B$  at  $t=160$ .

160

161 The pair of the layers is Alfvénic resonances indeed, which is demonstrated in  
 162 Figure 3. Figure 3b shows the distribution for the ratio of the local Alfvénic speed and  
 163 the flow velocity. The locations of the resonance layers are approximately at the  
 164 position where the ratio is equal to 1. There are no shocks formed outside the  
 165 reconnection region, which is consistent with the results in a high beta plasma, it is  
 166 unfavorable to the formation of the fast shocks [Shen *et al.*,2000]. The incompressible  
 167 approximation means that the plasma beta is large without a strong guide field  
 168 [Biskamp, 2000]. The reasons why there are no shocks are that the plasma flow  
 169 generated by the magnetic reconnection only weakly changes the initially imposed  
 170 shear flow because the Alfvénic resonance layers not only absorb the flow and  
 171 magnetic energies generated by magnetic reconnection, but also prevent the strong  
 172 shear flow from interacting with the magnetic islands.

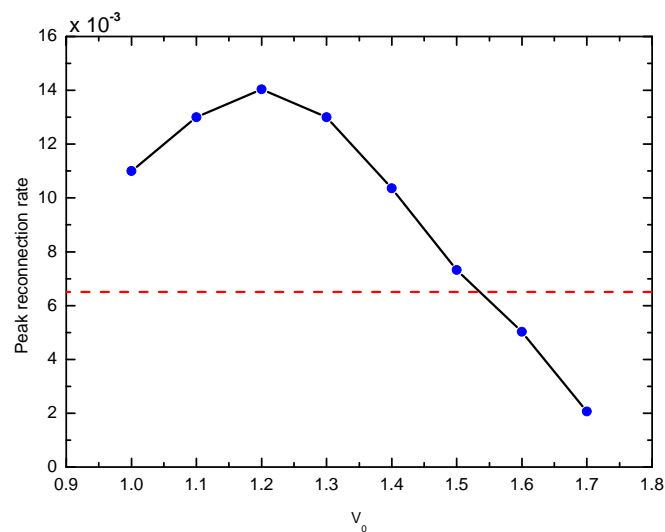


173  
 174 Figure 4. From left to right, the locations of Alfvénic Layers at the nearly saturated stage for  
 175 the fixed  $a_v = 4a_B$  cases with different shear velocities of  $v_0 = 1.2$ ,  $v_0 = 1.4$ , and  $v_0 = 1.6$ ,  
 176 respectively.

177  
 178 Figure 4 presents the locations of the Alfvénic resonance layers of three cases at  
 179 the same time  $t=140$  with fixed  $a_v = 4a_B = 0.8$  and different velocities  $v_0 = 1.2$ ,  
 180  $v_0 = 1.4$  and  $v_0 = 1.6$ , respectively. With the increase of the initial asymptotic flow



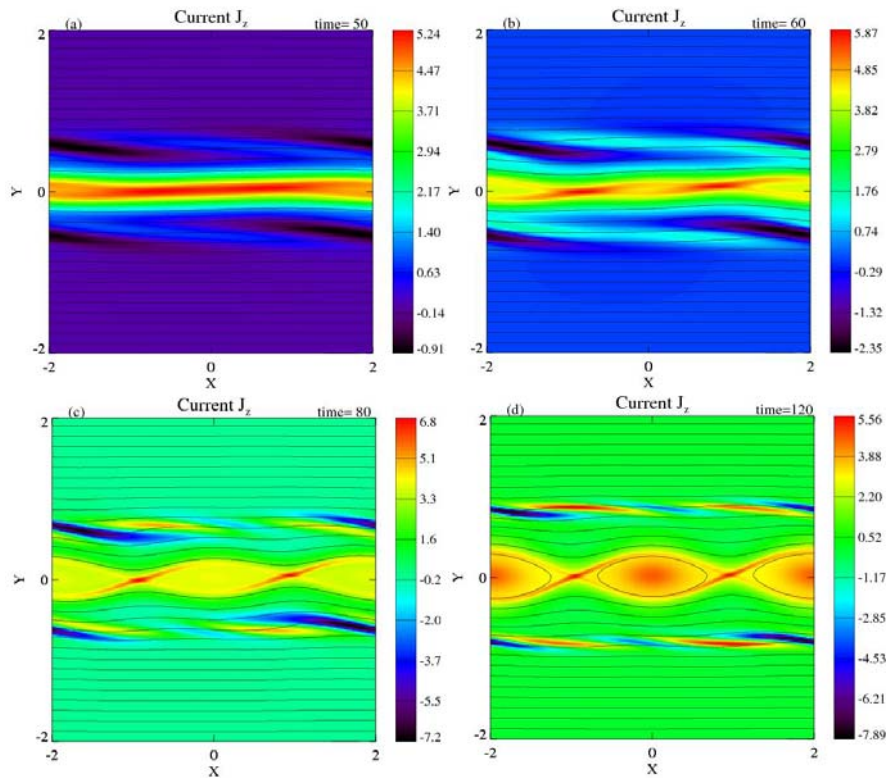
181 velocity  $v_0$ , it is clearly seen that the current intensity in the Alfvénic resonance  
 182 layers increases and the two resonance layers tend to be closer to each other. As the  
 183 asymptotic shear flow velocity increases, the initial location of the resonance layers  
 184 become closer to the current sheet as shown in Figure 1. The larger shear flow in the  
 185 narrower range has more free energy from initial shear flow to drive a larger  
 186 intensification of the current density in the Alfvénic resonance layers. The two closer  
 187 and stronger resonance layers that can be treated as the barriers prevent the growth of  
 188 the magnetic island. Therefore, the magnetic reconnection will be reduced as  $v_0$   
 189 increases for a given shear flow thickness as shown in Figure 5. The dashed line  
 190 represents the maximum reconnection rate for that case without the shear flow.



191  
 192 Figure 5. Peak reconnection rate related to different flow velocities for  $a_v = 0.8$ . The dashed  
 193 line indicates the peak reconnection rate for case without the shear flow.

194  
 195 Clearly, in Figure 5, there is a turning point at which the peak reconnection rate  
 196 begins to decrease with the increase of the shear velocity. As we know, KH instability  
 197 and properties of Alfvénic resonance layers could affect magnetic reconnection. When  
 198 the super-Alfvénic shear flow is less than  $v_0 \sim 1.2$ , the pair of Alfvénic layers is  
 199 weaker and located far away from each other, so the KH instability controls the

200 reconnection dynamics and enhances the growth of magnetic reconnection. Knoll and  
 201 Chacon have already shown the boosting effect with the initial imposed  
 202 super-Alfvénic shear flow as  $v_0$  increases [Knoll and Chacon 2002]. As the velocity  
 203 of the shear flow increases, the two resonance layers are located to close each other,  
 204 magnetic reconnection is largely suppressed due to formation of the Alfvénic  
 205 resonance layer. Therefore, the peak reconnection rate is reduced. Especially for the  
 206 case  $v_0 > 1.6$ , the reconnection rate drops below that without super-Alfvénic shear  
 207 flow, i.e., magnetic reconnection is suppressed by the super-Alfvénic shear flow,  
 208 which is never reported before.

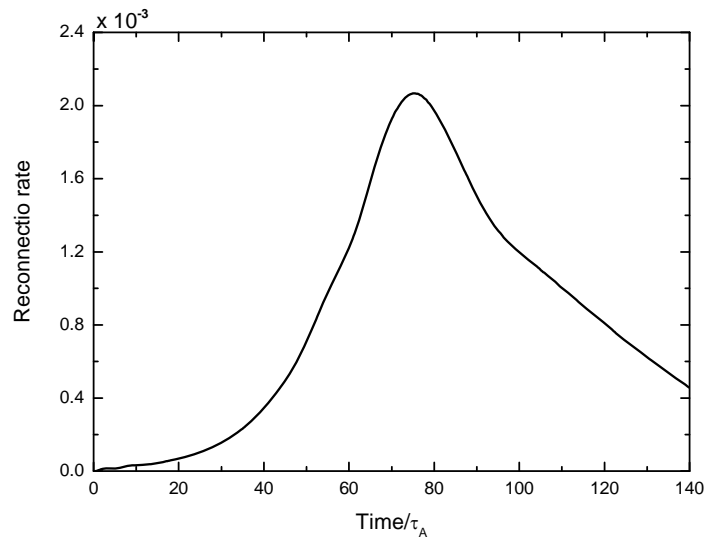


209  
 210 Figure 6. The evolution of the current density associated with magnetic field for  $v_0 = 1.7$  and  
 211  $a_v = 4a_B$ .

212

213 To further investigate the detailed mechanism of suppressing effects of  
 214 super-Alfvénic shear flow on magnetic reconnection, the time snapshots of the current  
 215 density with magnetic field lines for  $v_0 = 1.7$  and  $a_v = 4a_B$  are shown in Figure 6. It

216 is found that two magnetic islands emerge from the wavy current sheet. From the  
 217 relationship between the Alfvénic resonance layer and the asymptotic flow velocity  
 218 that has already analyzed in Figure 4, it is evidently shown that the separation of  
 219 Alfvénic resonance layers decreases with increase of the shear flow velocity. It is  
 220 clearly indicated that the closed distance of Alfvénic resonance layers can compress  
 221 and disturb the current sheet (Figure 6a), but largely suppress the  $m=1$  tearing mode  
 222 that is the most unstable mode without a shear flow. The compressed current sheet  
 223 leads to the development of the  $m=2$  tearing mode (Figure 6b). On the other hand, the  
 224 magnetic islands also modulate the structure of the Alfvénic resonance layers from the  
 225  $m=1$  mode to the  $m=2$  mode (Figure 6c). As the islands continue growing, the current  
 226 density in the Alfvénic resonance layers further intensifies. For the growth of  
 227 magnetic islands, it is necessary to push the resonance layers away from the  
 228 reconnection region. Subsequently, the reconnection develops more slowly in the case  
 229 with strong shear super-Alfvénic flow than with the weak shear super-Alfvénic flow  
 230 or without shear super-Alfvénic flow.



231  
 232 Figure 7. The time evolutions of the reconnection rates for  $v_0 = 1.7$  and  $a_v = 4a_B$ .

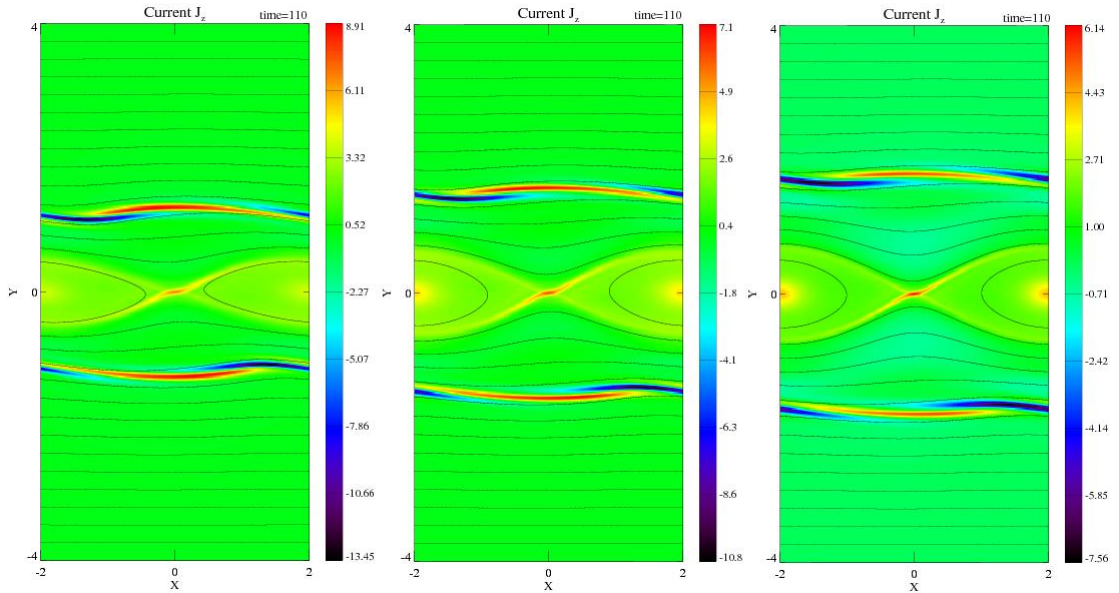
233  
 234 Figure 7 show the time evolutions of the reconnection rates for the two islands  
 235 situation ( $v_0 = 1.7, a_v = 0.8$ ). The two islands appear almost during the rapid growth

236 phase of the magnetic reconnection. The reconnection rate grows fast as the two  
 237 islands develop, then decreases as the islands gradually saturate. The peak  
 238 reconnection rate is much smaller than that for the small  $v_0$  cases mainly because the  
 239 Alfvénic resonance layers are closed to the reconnection current sheet and sufficiently  
 240 suppress the magnetic reconnection.

241

## 242 **B. Effects of shear flow thickness for $v_0 = 1.6$**

243 In this section, we mainly investigate the influence of the shear flow thickness on  
 244 magnetic reconnection and formation of resonance layers with fixing the shear flow  
 245 velocity  $v_0 = 1.6$ .



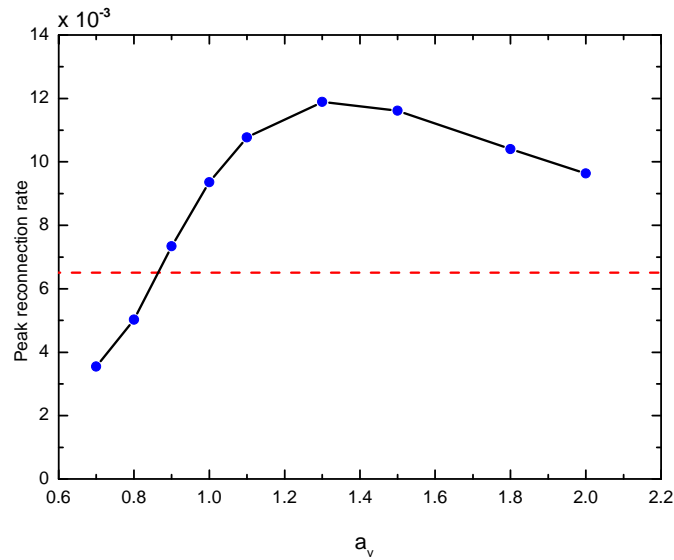
246

247 Figure 8. From left to right, locations of Alfvénic resonance layers at the saturated stage for  
 248 fixing flow velocity ( $v_0 = 1.6$ ) with different shear thickness of  $a_v = 0.8$ ,  $a_v = 1.0$ , and  
 249  $a_v = 1.4$ , respectively.

250

251 Figure 8 shows the same images as figure 4 for varied thickness of shear flow  
 252 ( $a_v = 0.8$ ,  $a_v = 1.0$  and  $a_v = 1.4$ , respectively) cases with fixed  $v_0 = 1.6$  at  $t=110$ .  
 253 From left to right of Figure 8, it is clearly to see the pair of Alfvénic resonance layers  
 254 tend to move away from each other and the current densities in the Alfvénic resonance

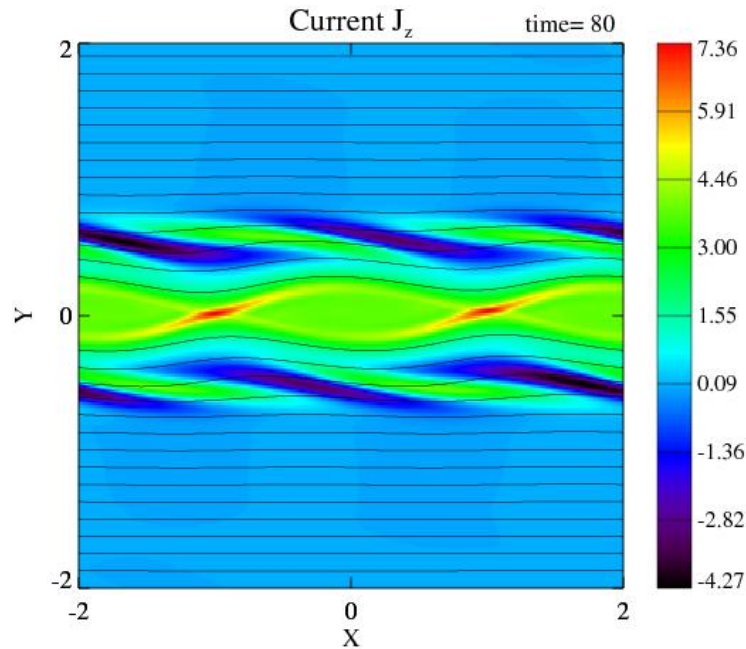
255 layers becomes weaker with the increase of the shear flow thickness. The initial  
 256 location of the resonance layers become closer to the central current sheet as the  
 257 decrease of the shear flow thickness or the increase of the initial asymptotic flow  
 258 velocity as illustrated in Figure 1. It is indicated that the two variables  $a_v$  and  $v_0$   
 259 have the similar role on the location of Alfvénic resonance layers. As the current  
 260 intensifications in Alfvénic resonance layers increase and its separation reduces, the  
 261 size of magnetic island become smaller. Therefore, the magnetic reconnection is  
 262 suppressed by a strong shear flow with the small  $a_v$  cases.



263  
 264 Figure 9. Peak reconnection rates related to different thicknesses of shear flow for  $v_0 = 1.6$ . The  
 265 dashed line indicates the peak reconnection rate for case without the shear flow.

266  
 267 Figure 9 shows the influence of different thickness  $a_v = 0.7 \sim 2.0$  of the shear  
 268 flow on peak reconnection rates for  $v_0 = 1.6$ . It is evident that a threshold for the  
 269 thickness of the shear flow exists. The peak reconnection rate is greater than that  
 270 without an initial shear flow, when the thickness of the shear flow is larger than  
 271  $a_v \sim 0.85$ . A maximum of the peak reconnection rate is obtained at  $a_v = 1.3$ , that is,  
 272 the boosting effect becomes strongest in this case. The reason why the peak

273 reconnection has such tendency is resulted from the competition between the  
 274 suppressing effects of Alfvénic resonances and the boosting effect of the  
 275 Kelvin-Helmholtz instability. The pair of Alfvénic resonance layers is far away from  
 276 each other with the increase of the thickness, the suppression of magnetic  
 277 reconnection become weaker, then the peak reconnection rate increases. When the  
 278 gradient of the shear velocity is weak in the region of the current sheet, the roles of  
 279 shear flows are gradually disappeared and the results are the same as that without an  
 280 initial shear flow. As a result, the peak reconnection rate goes down when  $a_v$  is  
 281 larger than 1.3.



282  
 283 Figure 10. Contour plots of the current density distribution for  $v_0 = 1.6$ ,  $a_v = 0.7$  at  $t=80$ .

284  
 285 When the thickness of the shear flow is narrow enough, for example  $a_v = 0.7$  as  
 286 shown in Figure 9, the peak reconnection rate is smaller than that without the shear  
 287 flow. It is clearly seen that the two magnetic islands emerge from the wavy current  
 288 sheet as shown in Figure 10 because the small separation distance of the resonance  
 289 layers largely reduces the reconnection rate. The detailed mechanism has already been  
 290 investigated in the case for  $v_0 = 1.7$  and  $a_v = 0.8$  in Section 3A. It's noteworthy that  
 291 two magnetic islands are generated when the peak reconnection rate is less than that

292 of the case without an initially imposed shear flow.

293

#### 294 **4. Summary and Discussion**

295 The influences of the super-Alfvénic shear flow on the tearing mode instability are  
296 carefully investigated with the resistive incompressible MHD model. It is found that  
297 Alfvénic resonance layers can form in the inflow region during the magnetic  
298 reconnection in the presence of super-Alfvénic shear flow. The Alfvénic resonance  
299 layers are located where the initial shear velocity equals to the local Alfvénic speed  
300 and drift away from the current sheet as the magnetic island develops. The intensity of  
301 the current density in the Alfvénic resonance layers is determined by the shear  
302 strength of the external shear flow, which depends on the initial asymptotic flow  
303 velocity and thickness of the shear flow, and the growth rate of the magnetic island.  
304 As the initial asymptotic flow velocity increases or the thickness of the shear flow is  
305 reduced, the two Alfvénic resonance layers approach each other and the suppressing  
306 effect of Alfvénic resonance layers is strengthened. When the thickness of the shear  
307 flow is thicker than that of the current sheet, magnetic reconnection with  
308 super-Alfvénic shear flow is mostly controlled by the Alfvénic resonance layers and  
309 the Kelvin-Helmholtz instability.

310 With a fixed thickness of the shear flow  $a_v = 0.8$ , in the parameter regime of the  
311 shear flow velocity below  $v_0 = 1.2$ , the Kelvin-Helmholtz resistive instability is the  
312 dominant process and the growth of magnetic reconnection increases with increase of  
313 the flow velocity. As the flow velocity is larger than  $v_0 = 1.3$ , the presence of the  
314 Alfvénic resonance layers mainly shows a suppressing effect on magnetic  
315 reconnection, and the peak reconnection rate decreases with increase of flow velocity.  
316 When the flow velocity further increases over  $v_0 \sim 1.5$ , the peak reconnection rate  
317 reduce below that without an initially imposed shear flow.

318 With a given flow velocity, there also exists a threshold for the thickness of the  
319 shear flow. The thresholds are different for different velocities of shear flow. For

320  $v_0 = 1.6$ , the threshold is  $a_v \sim 0.85$ . Below the threshold, the peak reconnection rate  
321 is less than that of the case without an initially imposed shear flow and two magnetic  
322 islands are usually generated due to formation of Alfvénic resonance layers near the  
323 central current sheet.

324

### 325 **Acknowledgement**

326 This work is supported by the National Natural Science Foundation of China under  
327 Grant No. 11175156 and 41074105, the China ITER Program under Grant No.  
328 2013GB104004 and 2013GB111004

329

### 330 **References**

- 331 Angelopoulos, V., J. P. McFadden, D. Larson, C. W. Carlson, S. B. Mende, H. Frey, T. Phan, D.  
332 G. Sibeck, K. H. Glassmeier, U. Auster, E. Donovan, R. I. Mann, I. J. Rae, C. T. Russell, A.  
333 Runov, X. Z. Zhou, L. Kepk (2008), Tail reconnection triggering substorm onset, *Science*,  
334 321, 931.
- 335 Biskamp, D. (2000), *Magnetic Reconnection in Plasmas*, Cambridge Univ. Press, Cambridge, UK.
- 336 Bellan, P.M. (1994), Alfvén ‘resonance’ reconsidered: exact equations for wave propagation  
337 across a cold inhomogeneous plasma, *Phys. Plasmas*, 1, 3523.
- 338 Chen, Q., A. Otto, and L.C. Lee (1997), Tearing instability, Kelvin-Helmholtz instability, and  
339 magnetic reconnection, *J. Geophys. Res.*, 102, 151.
- 340 Chen, X. L., and P. J. Morrison (1990a), Resistive instability with equilibrium shear flow, *Phys.*  
341 *Fluids B* 2(3), 495.
- 342 Chen, X. L. and P. J. Morrison (1990b), The effect of viscosity on the resistive tearing mode with  
343 the presence of shear flow, *Phys. Fluids B* 2 (11), 2575.
- 344 Dungey, J. W. (1961), Interplanetary magnetic field and the auroral zones, *Phys. Rev. Lett.*, 6, 47.
- 345 Giovanelli, R. G. (1946), A theory of chromospheric flares, *Nature*, 158, 81.
- 346 Hurricane, O. A., T. H. Jensen, and A.B. Hassam, Two-dimensional magnetohydrodynamics  
347 simulation of a flowing plasma interacting with an externally imposed magnetic field, *Phys.*  
348 *Plasmas*, 2, 6.
- 349 Knoll, D. A. and L. Chacon (2002), Magnetic reconnection in the two-dimensional  
350 Kelvin-Helmholtz instability, *Phys. Rev. Lett.*, 88, 21.
- 351 La Belle-Hamar, A.L., Z. F. Fu, and L.C. Lee (1988), A mechanism for patchy reconnection at the  
352 dayside magnetopause, *Geophys. Res. Lett.*, 15, 2.
- 353 Li, J. H. and Z. W. Ma (2010), Nonlinear evolution of resistive tearing mode with sub-Alfvénic  
354 shear flow, *J. Geophys. Res.*, 115, A09216, doi:10.1029/2010JA015315.
- 355 Li, J. H. and Z. W. Ma (2012), Roles of super-Alfvénic shear flows on Kelvin-Helmholtz and  
356 tearing instability in compressible plasma, *Phys. Scr.*, 86, 045503.
- 357 Liu, Z. X., and Y. D. Hu (1988), Local magnetic reconnection caused by vortices in the flow field,



358 Geophys. Res. Lett., 15, 8.  
359 Miura, A. (1982), Nonlinear evolution of the Magnetohydrodynamic Kelvin-Helmholtz instability,  
360 Phys. Rev. Lett., 49, 11.  
361 Ofman, L., X. L. Chen, P. J. Morrison and R.S. Steinolfson (1991), Resistive tearing mode  
362 instability with shear flow and viscosity, Phys. Fluids B, 3(6), 1364.  
363 Ofman, L., P. J. Morrison, and R. S. Steinolfson (1993), Nonlinear evolution of resistive tearing  
364 mode instability with shear flow and viscosity, Phys. Fluids B, 5, 376.  
365 Pu, Z. Y., M. Yei, and Z. X. Liu (1990), Generation of vortex-induced tearing mode instability at  
366 the magnetopause, J. Geophys. Res., 95, A7.  
367 Pu, Z. Y., P. T. Hou, and Z. X. Liu (1990), Vortex-induced tearing mode instability as a source of  
368 flux transfer events, J. Geophys. Res., 95, A11.  
369 Shen, C. and Z. X. Liu (1999), The coupling mode between Kelvin-Helmholtz and resistive  
370 instabilities in compressible plasmas, Phys. Plasmas, 6(7), 2883.  
371 Shen, C. and Z. X. Liu, T. S. Huang(2000), Shocks associated with the Kelvin-Helmholtz-resistive  
372 instability, Phys. Plasma, 7(7), 2842.  
373 Wang, X., A. Bhattacharjee, Z. W. Ma, C. Ren, C. C. Hegna, and J. D. Callen (1998), Structure  
374 and dynamics of current sheets at Alfvén resonances in a differentially rotating plasma, Phys.  
375 Plasmas, 5(6), 2291.  
376 Wu, L. N. and Z. W. Ma (2014), Linear growth rates of resistive tearing modes with sub-Alfvénic  
377 streaming flow, Phys. Plasmas, 21, 072105  
378 Zhang, X., L. J. Li, L. C. Wang, J. H. Li and Z. W. Ma (2011), Influences of sub-Alfvénic shear  
379 flows on nonlinear evolution of magnetic reconnection in compressible plasmas, Phys.  
380 Plasmas, 18(9), 092112.